

Supplementary Information

Non-Arrhenius Kinetics and Slowed-Diffusion Mechanism of Molecular Aggregation of a Rhodamine Dye on Colloidal Particles

Tímea Šimonová Baranyaiová,^{*ac} Róbert Mészáros,^{cd} Táňa Sebechlebská,^b and Juraj Bujdák^{*ab}

^a *Department of Hydrosilicates, Institute of Inorganic Chemistry, Slovak Academy of Sciences, 845 36 Bratislava, Slovakia. E-mail: timea.baranyaiova@savba.sk; juraj.bujdak@savba.sk*

^b *Department of Physical and Theoretical Chemistry, Faculty of Natural Sciences, Comenius University in Bratislava, 842 15 Bratislava, Slovakia*

^c *Department of Chemistry, Faculty of Education, J. Selye University, 945 01 Komárno, Slovakia*

^d *Laboratory of Interfaces and Nanosized Systems, Institute of Chemistry, ELTE Eötvös Loránd University, H-1117 Budapest, Hungary*

Experimental Section

E1. Materials and the preparation of rhodamine 123 / montmorillonite (R123/Mt) dispersions:

Rhodamine 123 (R123, CAS Number 62669-70-9) with laser-grade purity was purchased from Sigma-Aldrich (Steinheim, Germany) in the form of chloride salt. The sample of Na⁺-montmorillonite Kunipia F (Mt) with the structural formula $[(\text{Si}_{7.82}\text{Al}_{0.18})(\text{Al}_{3.19}\text{Fe}_{0.21}\text{Mg}_{0.52})\text{O}_{20}(\text{OH})_4] \cdot (\text{Na}_{0.84}\text{Ca}_{0.05}\text{K}_{0.01})^1$ was purchased from Kunimine Industries Co., Ltd. (Tokyo, Japan). All the solutions and colloidal dispersions were prepared using deionized water produced by the Merck Millipore Milli-Q system (Darmstadt, Germany).

An aqueous stock solution of R123 was prepared by dissolving a small amount of the dye in deionized water. Its standardization was carried out in accordance with the Lambert-Beer law, using the maximum values of the absorbance for the series of R123 solutions in ethanol (EtOH) (prepared by diluting a small amount of the R123 stock solution by EtOH) and published value of the molar absorption coefficient of R123 in EtOH at the wavelength of maximum absorbance ($\epsilon_{\text{max}} = 8.52 \times 10^4 \text{ mol}^{-1} \text{ dm}^3 \text{ cm}^{-1}$)². Aqueous solutions of R123 with the required dye concentration were prepared by dilution of the stock solution with water. Chemometric analysis (using the method of MCR) of a series of absorption spectra of various concentrated aqueous solutions of R123 confirmed, that dye molecular aggregates are not formed at the used dye concentrations.

Colloidal dispersions of Mt were prepared by dispersing the required amount of Mt powder in deionized water. The as-prepared suspension was homogenized in an ultrasonic bath for ≈ 20 min, and stirred overnight prior to the experiments.

Dispersions prepared in order to test the effect of temperature: The colloidal systems containing R123-loaded Mt particles with the concentration of R123 and Mt of $8.35 \times 10^{-6} \text{ mol dm}^{-3}$ and 0.418 g dm^{-3} , respectively, were prepared by mixing of an aqueous solution of R123 with a colloidal dispersion of Mt in equal volume. The ratio of the amount of R123 to the mass of Mt ($n_{\text{R123}}/m_{\text{Mt}}$ ratio) was kept constant at 0.02 mmol g^{-1} for all the investigated dispersions.

Dispersions prepared in order to test the effect of the concentration of components: The colloidal systems with a $n_{\text{R123}}/m_{\text{Mt}}$ ratio of 0.02 mmol g^{-1} were prepared using the above-described procedure, while the concentration of both reactants was 0.5, 0.75, and 1.25 times the original value of c_{R123} ($8.35 \times 10^{-6} \text{ mol dm}^{-3}$) and c_{Mt} (0.418 g dm^{-3}). The concentration of R123

and Mt in the reaction mixtures was in the range from $4.18 \times 10^{-6} \text{ mol dm}^{-3}$ to $1.04 \times 10^{-5} \text{ mol dm}^{-3}$ and from 0.209 g dm^{-3} to 0.523 g dm^{-3} , respectively.

E2. Electrophoretic mobility measurements:

After the quick initial homogenization of the R123/Mt dispersions, the samples were tempered in a Julabo Corio CD-B5 water bath (with a temperature stability of $\pm 0.03^\circ\text{C}$)^{int1} at the required temperature ($\theta = 25, 30, 35, 40, 45,$ and 50°C) for 2 hours. Subsequently, the cell was filled with the dispersion and placed to the thermostated cell holder of the instrument with a temperature accuracy of $\pm 0.1^\circ\text{C}$ ^{int2}. The mean velocity of the R123-loaded Mt particles (v_E) at a given electric field strength (E) was determined from the measured frequency shift of the scattered light due to the moving particles utilizing the M3-PALS technique of the Malvern Zetasizer Nano ZSP instrument. The mean electrophoretic mobility (u_ζ) was given from $u_\zeta = v_E/E$ relationship and it was converted to electrokinetic (zeta) potential (ζ) according to the Smoluchowski approximation of the Henry equation³:

$$u_\zeta = \frac{\zeta \varepsilon_r \varepsilon_0}{\eta}$$

where ε_0 and ε_r are the permittivities of the vacuum and the relative permittivity of the medium, respectively, and η is the viscosity of the medium at the given temperature. Using the same methodology, electrophoretic mobility measurements were performed at 25°C for the R123/Mt dispersions with different component concentrations. The control electrophoretic mobility measurements were realized for dye-free Mt dispersions with a concentration of 0.418 g dm^{-3} at the required temperatures, and for the colloids of Mt with different concentrations at 25°C .

E3. Dynamic light scattering (DLS) measurements:

DLS experiments for R123/Mt systems were carried out at 175° scattering angle by the back-scattering utility of Malvern Zetasizer Nano ZSP instrument using a 10 mW He-Ne laser at $\lambda = 633 \text{ nm}$. The measurements were carried out at six different temperatures ($\theta = 25, 30, 35, 40, 45,$ and 50°C). The temperature of the reactants was adjusted to the required value before their mixing in a conical tube. Immediately after the quick initial homogenization of the reaction mixture, the cell was filled with the dispersion and placed into the thermostated cell holder with a temperature accuracy of $\pm 0.1^\circ\text{C}$. The duration of the measurements was 3 h, while the autocorrelation function was recorded in every 5 min. The temperature of the dispersion was kept constant during the measurement.

The apparent mean diffusion coefficient (D_{app}) was derived from the CONTIN analysis of the normalized autocorrelation functions, and the apparent mean hydrodynamic (or Stokes) diameter of the particle (d_H) was determined from the Einstein-Stokes equation⁴:

$$D_{app} = \frac{k_B T}{3\pi\eta d_H}$$

where T is the temperature, k_B is the Boltzmann constant, and η is the viscosity of the medium. It should be noted that the shape of the bare and dye coated Mt particles resembles nanolayers rather than spheres⁵. Therefore, the apparent mean Stokes diameter values give only a qualitative measure of the smectite particles' size. However, the primary goal of the DLS measurements was to test a potential agglomeration of the particles, which can be accurately monitored by the relative changes of the d_H parameter with changing the temperature, concentration of the components or other parameters.

The recording of the changes in the mean count rate, size and diffusion coefficient distribution of the Mt particles during the formation of R123 molecular aggregates was controlled by the Malvern Zetasizer software. Using the same methodology, DLS measurements were performed at 25°C for the R123/Mt dispersions with different component concentrations. Control DLS experiments were performed for R123-free Mt dispersions with a concentration of 0.418 g dm⁻³ at the required temperatures, and for the Mt colloids with different concentrations at 25°C.

E4. Kinetics measurements of R123 molecular aggregation in Mt dispersions:

The absorption spectra of R123/Mt dispersions were recorded at 6 different temperatures (in the range from 25°C to 50°C with an interval of 5°C) after mixing of an aqueous solution of R123 with a colloidal dispersion of Mt in equal volume using a stopped-flow device (RX2000 Rapid Mixing Stopped-Flow Unit, Applied Photophysics Ltd., Leatherhead, UK). The temperature of the reactants was set to the desired value before the mixing. The same temperature was set for the thermostated cell holder of the spectrophotometer (89054A, Agilent Technologies, Waldbronn, Germany) with a temperature accuracy of $\pm 0.2^\circ\text{C}^{\text{int}3}$, where the quartz cell of the stopped-flow device (with a pathlength of 10 mm) was inserted. The measurements were initiated by a trigger that activated the recording of the spectra as soon as the reactants were injected from the syringes of the stopped-flow device into the cell.

Absorption spectra of the reaction mixtures were recorded using UV-Vis spectrophotometer Agilent 8453 (Agilent Technologies) over a wavelength range of 190 nm to 1100 nm. Spectral changes of R123 were recorded in kinetics mode for 3 hours. The diode array detector (DAD)

of the spectrophotometer enabled a rapid recording of the spectra over the entire wavelength range within a fraction of a second (approaching the shortest scan time of the detector, 0.1 s)^{int4}, while the scan time was set and controlled by the software of the spectrophotometer (Agilent ChemStation). After mixing of the reactants, the spectra were recorded every 1 s up to 600 s. After that, the time interval elapsed between the recordings of the spectra gradually increased by 5% of the previous value. The number of spectra recorded for each reaction mixture was 729.

For the R123/Mt dispersions with different component concentrations, the kinetics measurements were realized at 25°C using the above-described procedure.

E5. Baseline correction of the absorption spectra:

Prior to chemometric analysis, baseline correction of the R123 absorption spectra⁶ was performed in order to eliminate the effect of light scattering on the results of MCR analysis. In the first step, a nonlinear regression analysis of the selected part of recorded spectra (without the wavelength ranges that correspond to the absorption bands of R123) was performed in Gnuplot (version 5.2). The spectra were fitted using the function described by:

$$b(\lambda) = \sum_{k=3}^5 a_k \cdot \lambda^{-k}$$

where λ corresponds to the wavelength. Using the obtained values of the constants a_3 , a_4 and a_5 , the baseline was calculated over the entire wavelength range separately for each spectrum. In the last step, the calculated values of $b(\lambda)$ were subtracted from the respective absorption spectrum.

E6. Chemometric analysis of the absorption spectra:

The chemometric analysis was carried out using the method of Multivariate Curve Resolution (MCR) - Alternating Least Squares (Unscrambler software package, CAMO, Norway, Oslo). MCR analysis was performed for spectra obtained after baseline subtraction, over the wavelength range from 400 nm to 600 nm, which corresponds to the main absorption band of R123 in the visible (Vis) part of the spectra. Before the calculation, the spectra recorded for the R123/Mt systems at different temperatures were merged into one matrix. The size of the analysed spectral data matrix was $4,374 \times 201$. The application of the MCR algorithm⁷ led to their decomposition into the matrices of the spectral and concentration profiles ($\varepsilon_i(\lambda)$ and $c_i(t)$, respectively) of the different spectral forms of R123.

$$d(t,\lambda) = \sum_{i=1}^r c_i(t) \cdot \varepsilon_i(\lambda) + e(t,\lambda)$$

The meaning of the symbols is as follow:

- $d(t, \lambda)$ denotes spectral data matrix, and its elements correspond to the absorbance of R123 at the wavelength λ at time t elapsed from the mixing of the reactants.
- i represents the number of independent spectral forms of R123.
- $\varepsilon_i(\lambda)$ denotes the elements of the spectral profile matrix and expresses the dependence of the molar absorption coefficient of the respective spectral form of R123 on the wavelength.
- $c_i(t)$ denotes the elements of the concentration profile matrix and expresses the concentration of the respective spectral form of R123 as a function of time elapsed from the mixing of the reactants.
- $e(t, \lambda)$ represents the matrix of the residuals of the spectral data matrix decomposition.

The non-negativity constraint was applied for both the calculated spectral and concentration profiles. The usage of the MCR method enabled to determine the minimum number of different spectral species of R123 present in Mt dispersions (*i.e.* dye monomers and different types of molecular aggregates), for which the product of the concentration and spectral profile matrices allows the reconstruction of the measured spectral data matrix with sufficiently low residuals. The optimal number of R123 species was obtained by comparing the size and structure of the residuals of the spectral matrix decomposition considering the presence of different numbers of components. Only the components whose spectral profiles could be interpreted in accordance with the exciton theory were considered. Another restriction was that the calculated spectral profile of R123 adsorbed monomers should be identical to the shape of the spectrum of the R123 water solution.

The chemometric analysis of the R123 spectral data matrix obtained for the colloidal systems with different component concentrations (with the size of $2,916 \times 201$) was realized using the same calculation procedure and constraints.

E7. Calculation of real spectral and concentration profiles of R123 spectral species:

Elements of the concentration and spectral profile matrices, obtained by MCR analysis ($\varepsilon_i'(\lambda)$ and $c_i'(t)$, respectively) were expressed in arbitrary units. Their real values were calculated

using the method of multiple linear regression (MLR,) with OriginPro 9.1 software (OriginLab Corporation, Northampton, Massachusetts, USA) in accordance with the equation:

$$c(R123) = r_0 + \sum_i r_i \cdot c_i'(t)$$

Arbitrary values of the concentrations were fitted using the constant value of the sum concentration of R123 in the R123/Mt dispersions over the entire time range of the kinetics measurements. The intercept (r_0) was set to zero. Obtained values of the regression coefficients (r_i) were used to calculate the real values of the concentration and molar absorption coefficient of the respective R123 species as shown in the equations below:

$$c_i(t) = r_i \cdot c_i'(t)$$

$$\varepsilon_i(\lambda) = \frac{\varepsilon_i'(\lambda)}{r_i}$$

E8. Characterization of R123 molecular aggregates:

The energy difference between the H- and J-band of R123 molecular aggregates (in cm^{-1}) was calculated using the equation:

$$\Delta\tilde{\nu} = 10^7 \cdot \left(\frac{1}{\lambda_{\max}(\text{H-band})} - \frac{1}{\lambda_{\max}(\text{J-band})} \right)$$

where $\lambda_{\max}(\text{H-band})$ and $\lambda_{\max}(\text{J-band})$ correspond to the wavelength of the maximum intensity of the respective absorption band in the spectral profile of the aggregate.

The angle between the transition dipole moments of the interacting R123 cations in molecular aggregates (α) was calculated using the equation below^{8,9}.

$$\alpha = \frac{360^\circ}{\pi} \cdot \arctan \sqrt{\frac{A_{\text{J-band}}}{A_{\text{H-band}}}}$$

Symbols $A_{\text{J-band}}$ and $A_{\text{H-band}}$ denote the integrated area assigned to the respective absorption bands of the aggregate calculated in OriginPro 9.1 software.

The value of the slip angle (θ) corresponding to the angle between the main molecular axis of R123 cations and the centerline of the interacting dye molecules in the aggregate was calculated based on the equation:

$$\theta = \frac{180^\circ - \alpha}{2}$$

E9. Calculation of the extent of R123 molecular aggregation and evaluation of kinetics parameters of the formation of R123 J-aggregates:

The fraction of R123 cations participating in the formation of H- and J-type of aggregates at the beginning of the reaction and after reaching the equilibrium state (*i.e.* the initial and final extent of R123 H- and J-aggregation, designated as p_i and p_f of the respective species) was calculated as the ratio of the concentration of dye cations forming the respective type of molecular aggregates to the total dye concentration corresponding to the first and last value of the respective concentration profile.

Kinetics parameters of R123 J-aggregation were calculated from the results of nonlinear regression analysis of their real concentration profiles using OriginPro 9.1 software. Fitting of the concentration profiles was performed using two-phase exponential growth function^{10,11}:

$$c_{J-agg}^\infty - c_{J-agg}(t) = c_1 \cdot e^{-k_1 \cdot t} + c_2 \cdot e^{-k_2 \cdot t}$$

Symbols $c_{J-agg}(t)$ and c_{J-agg}^∞ denote the concentration of R123 cations forming J-aggregates at time t elapsed from the mixing of the reactants, and after the reaching of equilibrium state ($t \rightarrow \infty$), respectively. k_1 , k_2 and c_1 , c_2 represent the rate constants and the concentrations of dye cations that participate in the formation of J-aggregates through the respective reaction processes. The relationship used to calculate the extrapolated concentration of R123 molecules forming J-aggregates at time zero (c_{J-agg}^0) is given below:

$$c_{J-agg}^0 = c_{J-agg}^\infty - (c_1 + c_2)$$

The averaged half-life of J-aggregation ($t_{1/2}$) was obtained from the performed fit on J-aggregates concentration profiles as the time required to reach the concentration defined below:

$$c_{J-agg}^{t_{1/2}} = c_{J-agg}^0 + \frac{c_{J-agg}^\infty - c_{J-agg}^0}{2}$$

E10. Calculation of single-exponential growth curves:

The curves corresponding to the fast and slow process of R123 J-aggregation were simulated in OriginPro 9.1 software based on the functions below and using the obtained values of dye molecular aggregation kinetics parameters summarized in Table 1.

$$c_{J-agg}^{\infty}(\text{fast process}) - c_{J-agg}(t) = c_1 \cdot e^{-k_1 \cdot t}$$

$$c_{J-agg}^{\infty}(\text{slow process}) - c_{J-agg}(t) = c_2 \cdot e^{-k_2 \cdot t}$$

Results

S1. Results of the electrophoretic mobility and DLS measurements

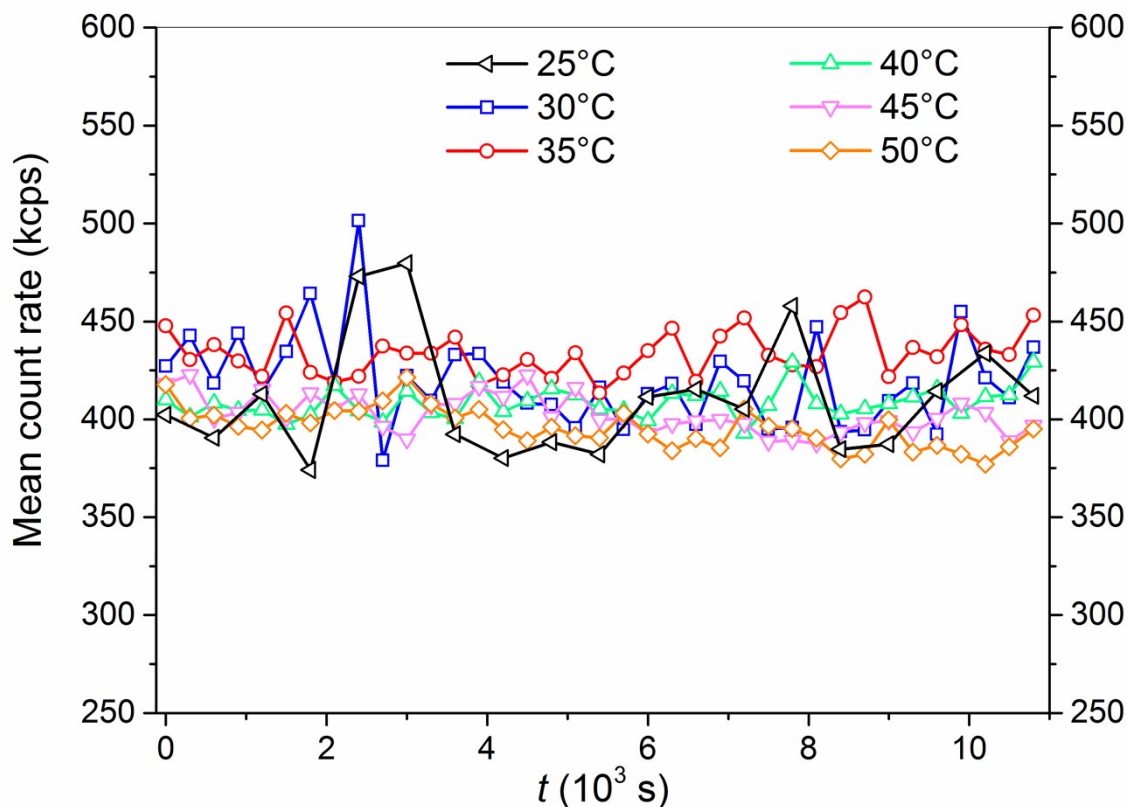
The apparent mean zeta potential (ζ) of Mt particles before and after the addition of dye cations were measured at six temperatures (Table S1). ζ values were not largely dependent on the temperature within the experimental error. The averaged value of the zeta potential of R123/Mt particles was less negative ($\zeta_{av} = -38 \pm 2$ mV) than that of the non-modified Mt particles ($\zeta_{av} = -45 \pm 1$ mV). The difference between these two values is small but statistically significant ($P < 0.0001$). This small difference was attributable to the low amount of adsorbed cationic dye molecules (0.02 mmol g^{-1}), which compensated the negative electrokinetic charge of the particles. As indicated above, the amount of dye cations in the R123/Mt colloidal systems represented only 1.75% with respect to the cation exchange capacity of the Mt particles ($\text{CEC} = 1.14 \text{ mmol g}^{-1}$)¹⁰, and the change in particle zeta potential as observed after the addition of the dye should not cause colloidal destabilization. As shown in Fig. S1, the scattered intensity of the Mt/R123 dispersions was found to be constant at all investigated temperatures within 3 h from the onset of mixing of the dye solution and Mt particles. As shown in Table S1, d_H of Mt particles was dependent neither on the temperature nor on the presence of R123 molecules.

Table S1 Values of the apparent mean zeta potential (ζ) and the apparent mean Stokes diameter (d_H) of the silicate particles obtained for dispersions of the non-modified (left side) and R123-loaded (right side) Mt at different temperatures (θ).

θ (°C)	Mt dispersion ^a		Mt/R123 dispersion ^b	
	ζ (mV)	d_H (nm)	ζ^c (mV)	d_H^d (nm)
25	-43 ± 2	240 ± 10	-39 ± 1	230 ± 10
30	-43 ± 1	260 ± 10	-38 ± 1	250 ± 10
35	-45 ± 3	255 ± 15	-38 ± 1	270 ± 10
40	-46 ± 1	260 ± 10	-37 ± 1	290 ± 15
45	-45 ± 1	270 ± 10	-38 ± 1	245 ± 10
50	-46 ± 1	280 ± 10	-40 ± 1	250 ± 15

^a The concentration of Mt was $4.18 \times 10^{-1} \text{ g dm}^{-3}$. ^b The concentration of Mt and the n_{R123}/m_{Mt} ratio was $4.18 \times 10^{-1} \text{ g dm}^{-3}$ and 0.02 mmol g^{-1} , respectively. ^c The values were recorded after approximately 2 h from the preparation of Mt/R123 dispersions. ^d The average of the values recorded during the 3 h DLS measurements.

Fig. S1 Time evolution of the intensity of the scattered light for the R123/Mt dispersions with n_{R123}/m_{Mt} ratio of 0.02 mmol g^{-1} ($c_{R123} = 8.35 \times 10^{-6} \text{ mol dm}^{-3}$ and $c_{Mt} = 0.418 \text{ g dm}^{-3}$) at different temperatures.



S2. Spectral properties of R123 solutions

For the aqueous solution of R123, a narrow and intense absorption band was recorded in the wavelength range from 400 nm to 560 nm, which is characteristic of the monomeric form of R123. The maximum value of the absorbance occurs at 500 nm (λ_{max}). The light absorption of R123 in the visible range is due to $\pi - \pi^*$ electronic transition of the xanthylium chromophore¹². The presence of a low-intensity shoulder approximately at 470 nm is related to a vibronic transition $1 \leftarrow 0$ ¹³.

First, the impact of temperature on the absorption spectra of the dye solution without Mt ($c_{R123} = 8.35 \times 10^{-6} \text{ mol dm}^{-3}$) was investigated. The effect was negligible showing a slight decrease in the maximum intensity and an increase in the spectral bandwidth of the main band with increasing temperature (not shown). The difference between the maximum absorbance of the dye at 50°C and 25°C was 2.4×10^{-2} representing 4.6% of the maximal absorbance at 25°C ($A_{500\text{nm}} = 0.53$). In summary, the changes in R123 spectra with temperature were not significant.

S3. Spectral changes of R123 in Mt dispersions

The observed changes can be summarized in the following points:

- Bathochromic shift of the main absorption band of R123 with the magnitude of 7 nm was detected in the 1st spectrum, recorded after 0.5 s from the mixing of the reactants (Fig. S2, blue arrow). The shift indicates an increase in the polarity of the environment of R123 molecules due to their adsorption onto a basal surface of Mt particles¹⁴. This observation confirms that the adsorption of R123 cations is a very fast process. According to previous observations¹⁵, the kinetics of the adsorption is controlled by the rate at which dye cations diffuse from the bulk solution to the surface of the colloidal particles ($k_{\text{dif}} \sim 10^9 \text{ mol}^{-1} \text{ dm}^3 \text{ s}^{-1}$)⁴. At such a high value of adsorption rate constant, dye cations are initially adsorbed on the surface of smectite particles they reach first¹⁰.
- Spectral changes of R123 at longer times were associated with a gradual decrease in the intensity and an increase in the bandwidth of the main absorption band of R123. Absorbance increase at shorter and longer wavelengths was also observed (Fig. S2). The changes in the shape of the absorption spectrum of R123 indicate the formation of dye molecular aggregates.

Fig. S2 Second derivative absorption spectra of R123 in an aqueous solution (dashed line) and in a dispersion of dye coated Mt particles recorded at various time points (0.5 s, 2 min, 10 min, 30 min, and 3 h) after mixing the reactants (solid lines). The spectra were recorded at 25°C for R123-loaded Mt colloids with the concentration of R123 and n_{R123}/m_{Mt} ratio of 8.35×10^{-6} mol dm^{-3} and 0.02 mmol g^{-1} , respectively.

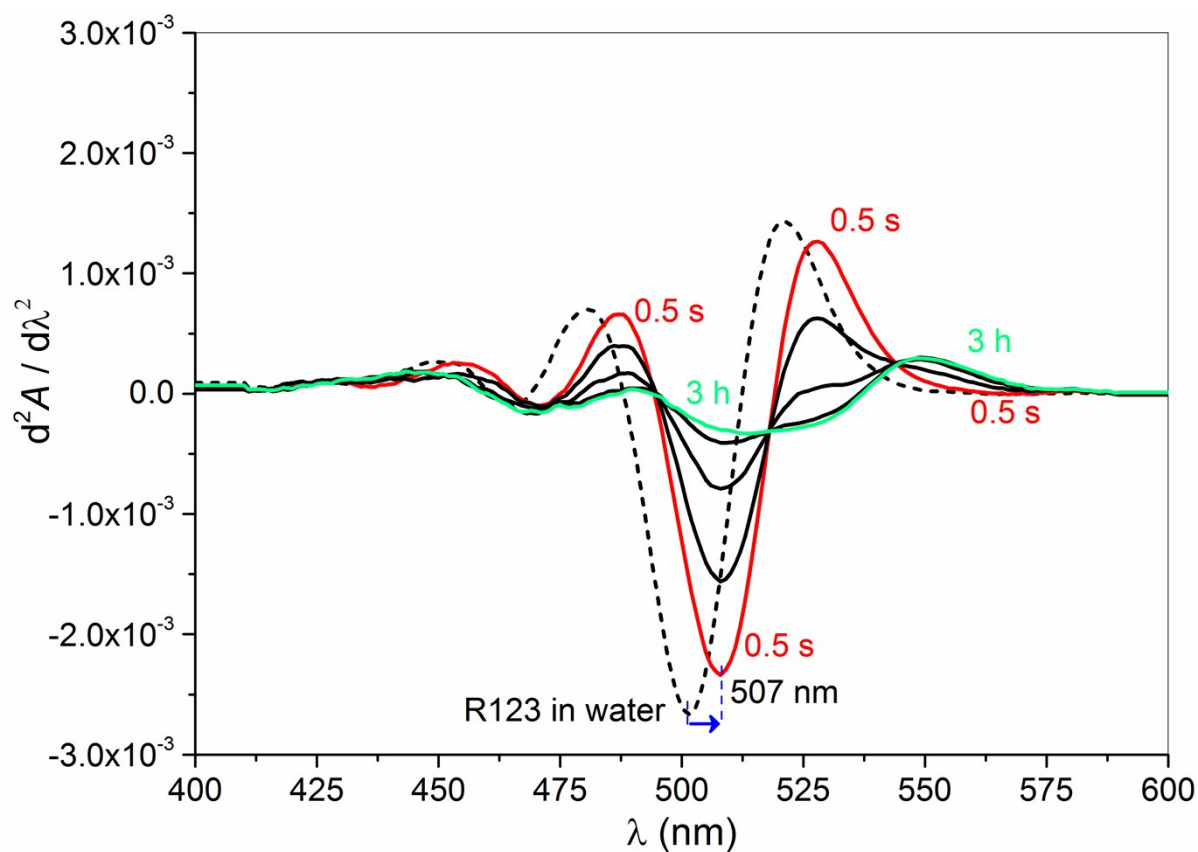
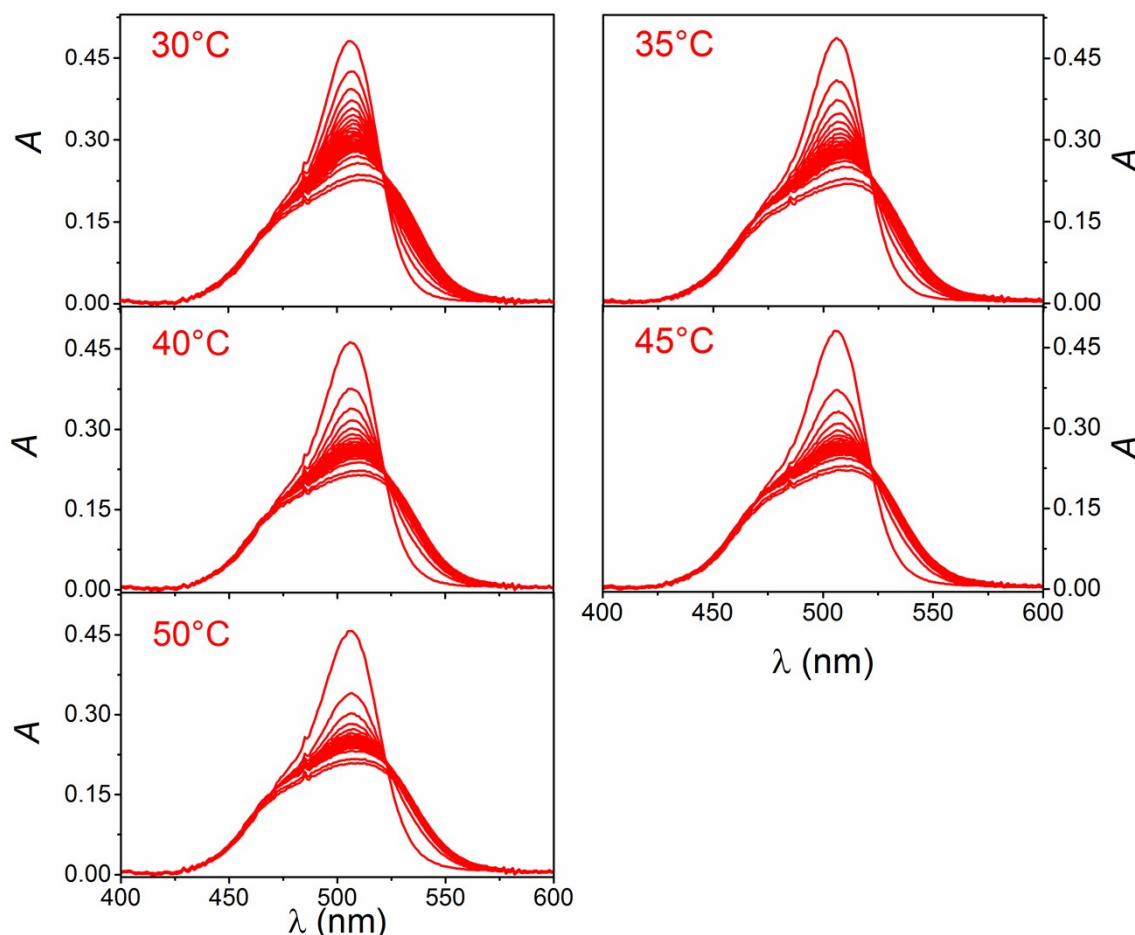


Fig. S3 Time evolution of R123 spectra in Mt dispersion during a 3-hour kinetics measurement at different temperatures. Every 30th recorded spectrum is shown after eliminating the effect of light scattering on Mt particles. The spectra were recorded for R123-loaded Mt colloids with the concentration of R123 and n_{R123}/m_{Mt} ratio of $8.35 \times 10^{-6} \text{ mol dm}^{-3}$ and 0.02 mmol g^{-1} , respectively.



S4. Details on the structure of R123 aggregates

For the oblique J-aggregates of R123, higher intensity ($\epsilon_{\max} = 3.45 \times 10^4 \text{ mol}^{-1} \text{ dm}^3 \text{ cm}^{-1}$) and narrower shape was observed for the red-shifted J-band of the aggregate. The energy difference between the H- and J-band was 2061 cm^{-1} . The magnitude of the angle between the transition dipole moments of the R123 cations (designated as α), which characterizes the mutual arrangement of the associated R123 molecules in the oblique J-aggregate, was 100.1° . The corresponding value of the slip angle was $\theta=39.9^\circ$.

In the case of twisted H-aggregates, the small value obtained for the angle between the transition dipole moments ($\alpha=12.2^\circ$) indicates the tight arrangement of the associated R123 molecules in the aggregate. The energy difference between the H- and J-band was 1950 cm^{-1} .

Fig. S4 Comparison of the fraction of R123 cations (p_i , p_f) found in the form of adsorbed monomers, and involved in the formation of oblique J-aggregates and twisted H-aggregates in dispersions of Mt with different temperatures (a) at the beginning ($t = 0.5$ s) of the kinetic measurements and (b) after reaching the equilibrium state. The concentration of R123 and the ratio of n_{R123}/m_{Mt} in the dispersions was 8.35×10^{-6} mol dm $^{-3}$ and 0.02 mmol g $^{-1}$, respectively.

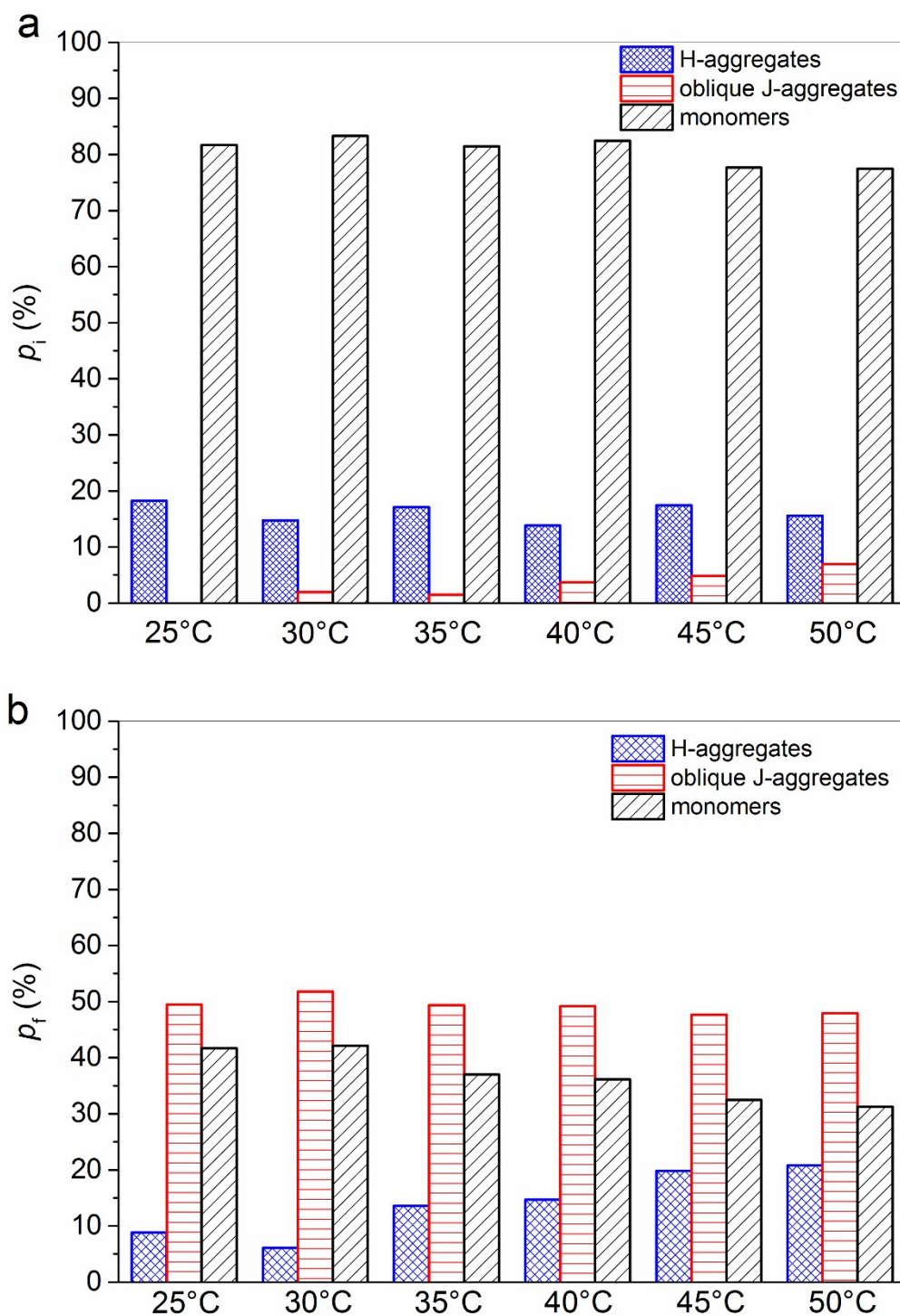


Fig. S5 Results of the regression analysis of the concentration profiles of R123 J-aggregates using the first-order, second-order, and two-phase exponential growth model (upper panel, R^2 corresponds to a coefficient of determination) and the comparison of the obtained residual profiles (lower panel) in Mt/R123 dispersions (a) at 25°C and (b) at 50°C. The concentration of R123 and the ratio of n_{R123}/m_{Mt} in the dispersions was $8.35 \times 10^{-6} \text{ mol dm}^{-3}$ and 0.02 mmol g^{-1} , respectively.

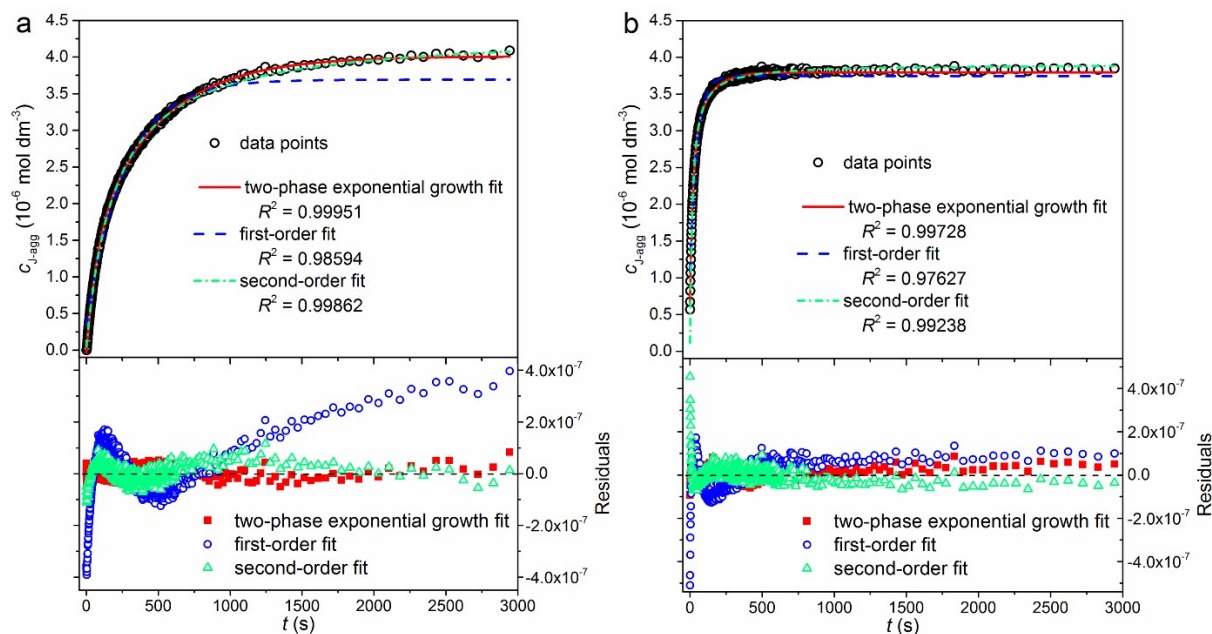


Table S2 Dependence of the diffusion coefficient of R123-loaded Mt particles on temperature obtained for the dispersions with a Mt concentration and n_{R123}/m_{Mt} ratio of 0.418 g dm⁻³ and 0.02 mmol g⁻¹, respectively.

θ (°C)	D^a ($\mu\text{m}^2 \text{s}^{-1}$)
25	2.1 ± 0.1
30	2.3 ± 0.2
35	2.5 ± 0.1
40	2.8 ± 0.1
45	3.2 ± 0.1
50	3.4 ± 0.2

^aThe average of the values recorded during the 3 h DLS measurements.

S5. Analysis of the conditions under which the Eyring-Polanyi equation (Equation 2) and Equation 3 show a linear dependence

$$k = \frac{\kappa \cdot k_B \cdot T}{h} \cdot e^{\frac{\Delta S^\ddagger}{R}} \cdot e^{-\frac{\Delta H^\ddagger}{RT}} \quad (2)$$

$$k = C + A \cdot T \cdot e^{\frac{B}{T}} \quad (3)$$

Linearity is mainly expressed by the entropic term $A \cdot T$, and the deviation from linearity is expressed by the enthalpy term $e^{\frac{B}{T}}$. Since the change in the enthalpy of molecular aggregation is negligible, it holds that $\Delta H^\ddagger \ll RT$, and the enthalpy term probably has a negligible effect on the functional dependence $k = f(T)$, making it appear to be linear. The B/T ratio is close to zero and $e^{\frac{B}{T}}$ is approximately 1. The Eyring-Polanyi relation only applies to a certain range of temperatures that are realistic for a given reaction taking place in aqueous colloidal systems. It cannot be extrapolated to infinite or zero temperature, therefore the constant C was also included in Equation 3.

Table S3 Regression parameters (A , B , C) and coefficient of determination (R^2) obtained by nonlinear regression analysis (using Equation 3) of the temperature dependence of the rate constants (k_1 a k_2) for the faster and slower formation of R123 J-aggregates.

	A ($\text{K}^{-1} \text{s}^{-1}$)	B (-)	C (s^{-1})	R^2
Fast process $k_1 = f(T)$	$1.390 \times 10^{-3} \pm 1.3 \times 10^{-5}$	0.88 ± 0.07	-0.402	0.9997
Slow process $k_2 = f(T)$	$2.9 \times 10^{-4} \pm 2 \times 10^{-5}$	-1.5 ± 0.5	-0.085	0.9806

Fig. S6 (a) Dependence of the enthalpy term in Eyring equation on temperature for the fast and slow process of R123 J-aggregation in Mt dispersions. (b) Temperature dependence of the Gibbs free energy of activation for the fast and slow process of R123 J-aggregation, calculated on the basis of the relationship $\Delta G^\ddagger = \Delta H^\ddagger - T \cdot \Delta S^\ddagger$.

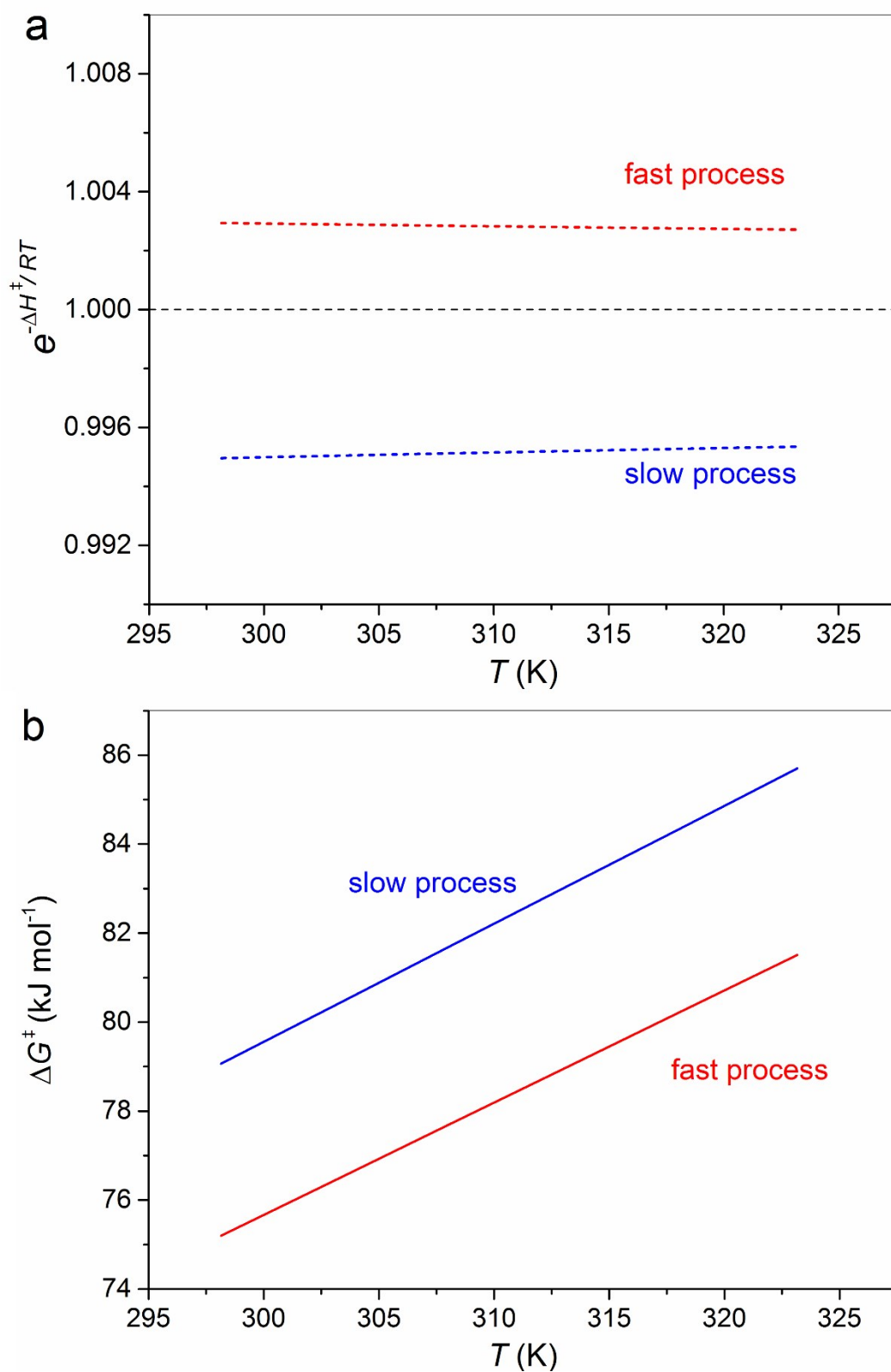


Table S4 Determined values of the rate constant of the fast and slow process of R123 J-aggregation in Mt dispersion at 5 and 10°C. The results were obtained for the systems with n_{R123}/m_{Mt} ratio and R123 concentration of 0.02 mmol g⁻¹ and 8.35×10⁻⁶ mol dm⁻³, respectively.

θ (°C)	k_1 (10 ⁻³ s ⁻¹)	k_2 (10 ⁻³ s ⁻¹)
5	1.73 ± 0.1	0.106 ± 0.03
10	2.36 ± 0.1	0.276 ± 0.002

Table S5 (a) Regression parameters (A , B , C) and coefficient of determination (R^2) of the nonlinear regression analysis (using Equation 3) of the temperature dependence of the rate constants (k_1 a k_2) for the fast and slow process of the formation of R123 J-aggregates and (b) calculated values of the activation enthalpy and entropy (ΔH^\ddagger , ΔS^\ddagger) of the respective processes, obtained for the extended temperature range from 5°C to 50°C.

a)

	A (K ⁻¹ s ⁻¹)	B (-)	C (s ⁻¹)	R^2
Fast process $k_1 = f(T)$	4.490×10 ⁻³ ± 4.7×10 ⁻⁴	270.5 ± 3.3	-3.3 ± 0.4	0.9958
Slow process $k_2 = f(T)$	9.4×10 ⁻⁴ ± 2×10 ⁻⁴	271.2 ± 7.8	-0.692 ± 0.2	0.9750

b)

	ΔH^\ddagger (J mol ⁻¹)	ΔS^\ddagger (J K ⁻¹ mol ⁻¹)
Fast process	2248 ± 28	-242 ± 25
Slow process	2255 ± 65	-255 ± 64

Table S6 Values of the apparent mean Stokes diameter (d_H) and diffusion coefficient (D) of the silicate particles obtained for dispersions of the non-modified (left side) and R123-loaded (right side) Mt particles with different concentrations.

c_{Mt} (g dm ⁻³)	Mt dispersion		Mt/R123 dispersion ^a	
	d_H (nm)	D (μm ² s ⁻¹)	d_H (nm)	D^b (μm ² s ⁻¹)
0.418	240 ± 10	2.1 ± 0.1	230 ± 10	2.1 ± 0.1
0.523	255 ± 30	2.0 ± 0.2	340 ± 10	1.4 ± 0.1

^a The n_{R123}/m_{Mt} ratio was 0.02 mmol g⁻¹. ^b The average of the values recorded during the 3 h DLS measurements.

Fig. S7 Real concentration profiles of R123 monomers and dye cations forming oblique J-aggregates obtained as a result of the decomposition of the R123 spectral data matrix recorded for Mt dispersions with an n_{R123}/m_{Mt} ratio of 0.02 mmol g⁻¹ but at different analytical concentrations of the components using the method of MCR. The values in μM correspond to a dye concentration in the R123/Mt systems, and the profiles assigned to the individual reaction mixtures are arranged in succession to provide better clarity.

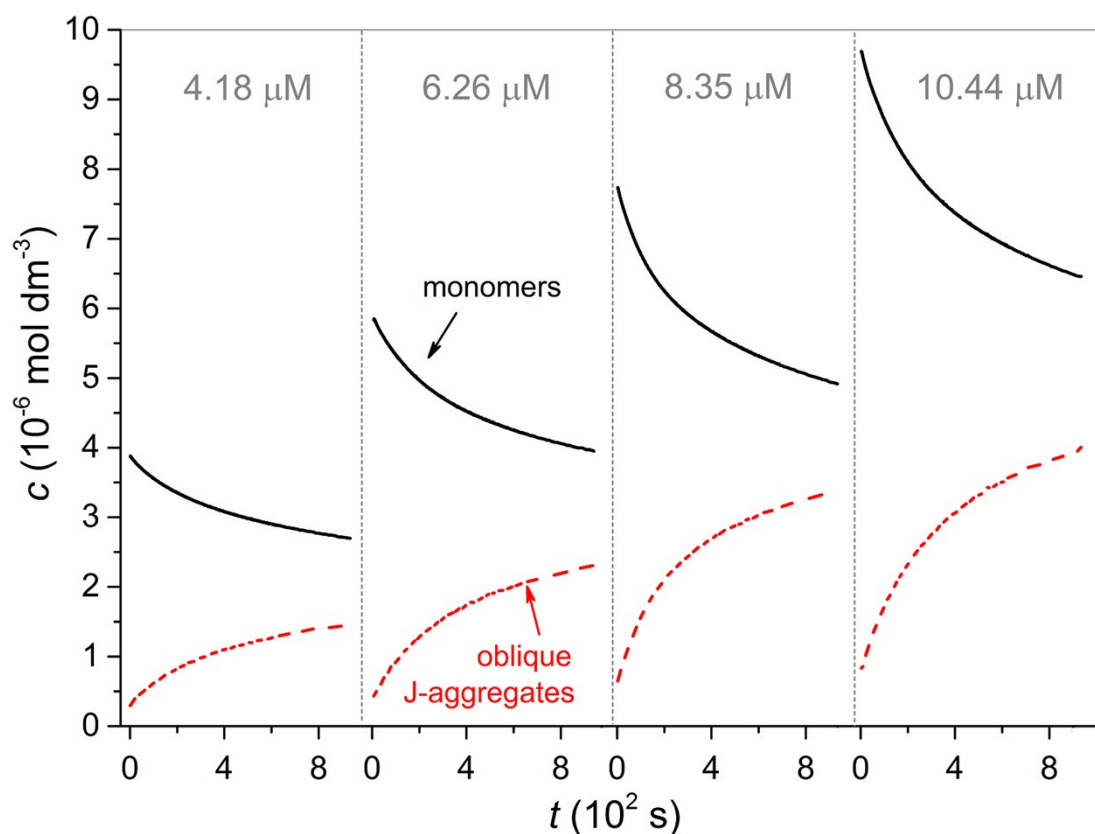


Table S7 Parameters of the kinetics of the formation of R123 oblique J-aggregates in Mt dispersions with the same $n_{\text{R123}}/m_{\text{Mt}}$ ratio (0.02 mmol g⁻¹) but at different analytical concentrations of the components.

c_{R123} ($\mu\text{mol dm}^{-3}$)	$c_{\text{J-agg}}^0 / c_{\text{J-agg}}^\infty$ ^a ($\mu\text{mol dm}^{-3}$)	c_1 / c_2 ^b ($\mu\text{mol dm}^{-3}$)	k_1 ^c (10^{-3} s^{-1})	k_2 ^c (10^{-3} s^{-1})	$t_{1/2}$ ^d (s)	$\Delta p_{\text{J-agg}}$ ^e (%)	R^2 ^f
4.18	0.299 / 1.63	0.150 / 1.18	11.72 ± 1.1	2.00 ± 0.07	284	31.8	0.9993
6.26	0.425 / 2.67	0.595 / 1.65	6.61 ± 0.6	1.57 ± 0.20	291	35.9	0.9995
8.35	0.615 / 3.83	1.047 / 2.16	8.90 ± 0.2	1.68 ± 0.08	228	38.5	0.9998
10.44	0.784 / 4.55	0.784 / 2.88	8.68 ± 0.4	1.89 ± 0.08	261	35.1	0.9998

The model of two-phase exponential growth function shown in Equation 1 was used. ^a R123 concentration used for the formation of J-aggregates at the initial state and after reaching the equilibrium in the reaction. ^b Concentration spans of the fast and slow process. ^c The rate constant of the fast and slow process. ^d The total half-life. ^e The difference in the extent of the formation of J-aggregates between the initial state and after reaching spectral equilibrium. ^f The coefficient of determination of the fit.

Fig. S8 Dependence of the rate constants of the faster and slower process of R123 J-aggregates formation (k_1 and k_2) on the concentration of Mt particles in R123/Mt dispersions. The values on the upper horizontal axis correspond to the concentration of R123 in the dispersions.

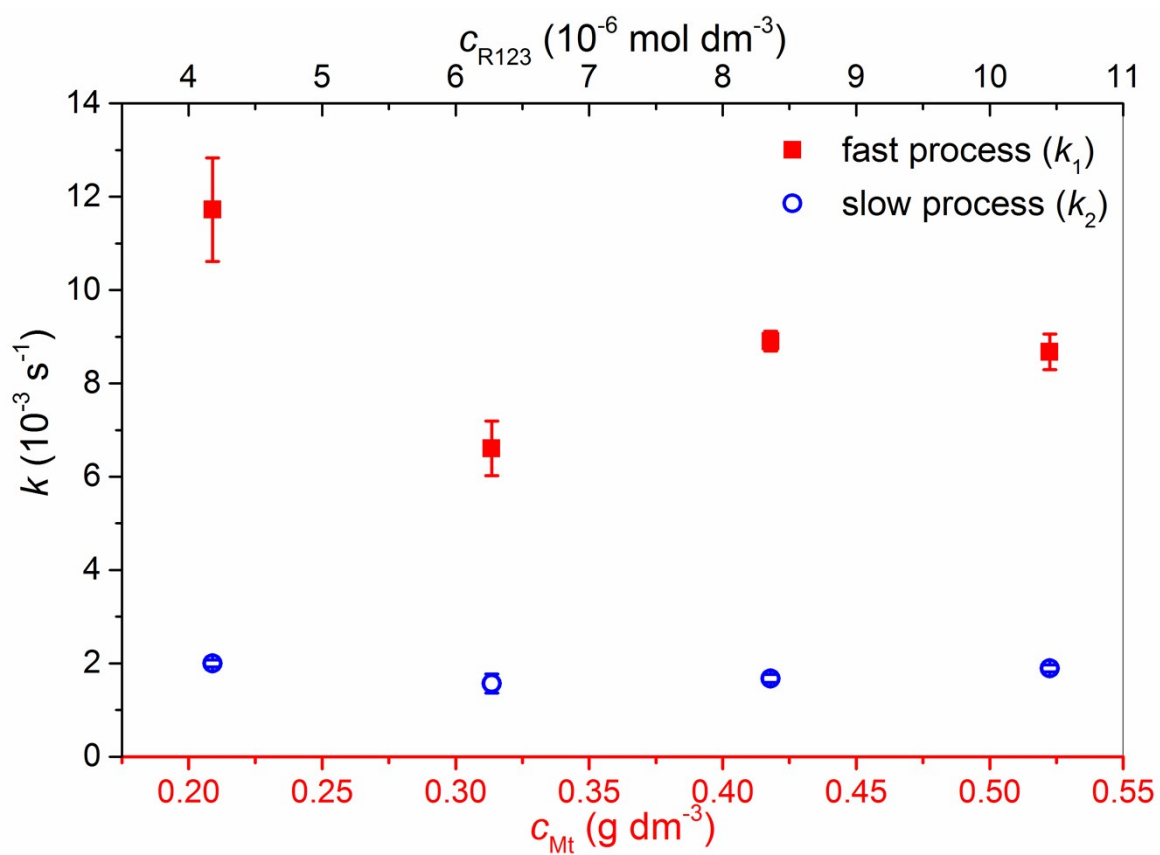
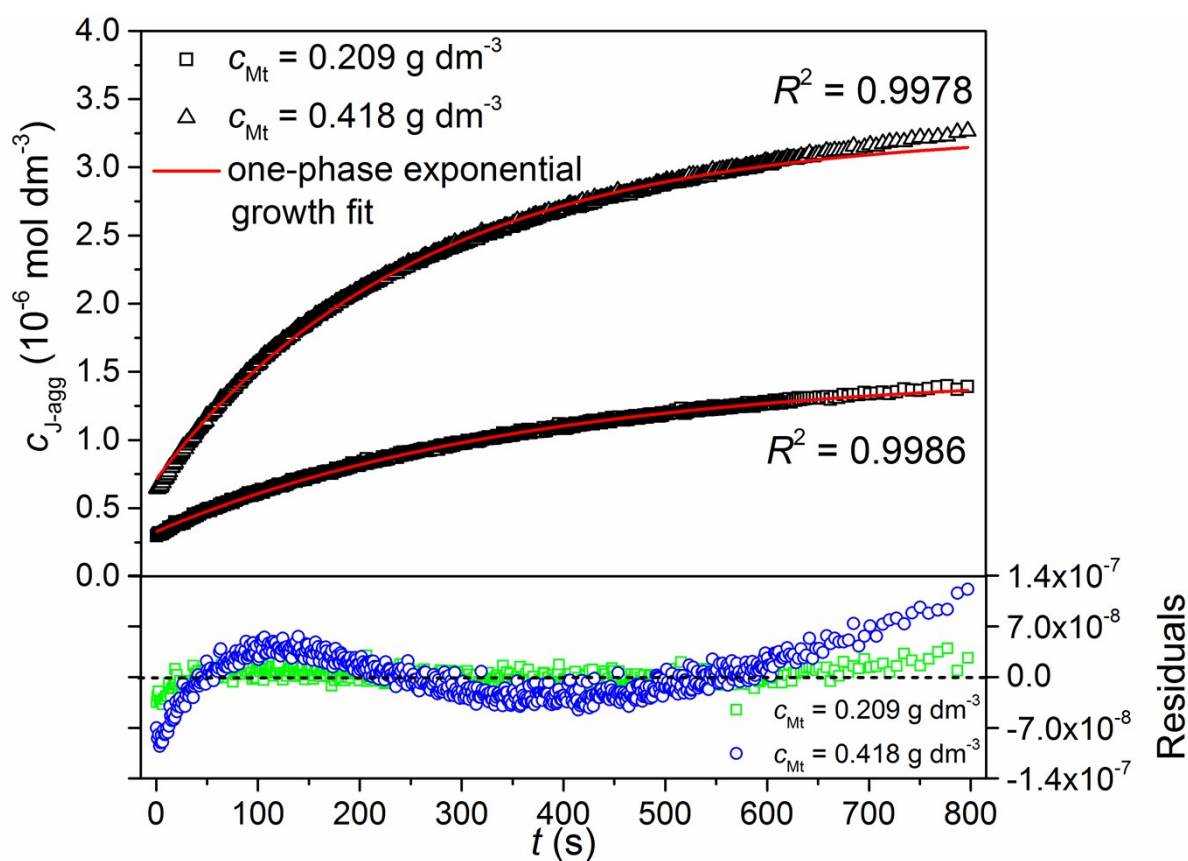


Fig. S9 Results of the regression analysis of the concentration profiles of R123 J-aggregates using one-phase exponential growth model (upper panel, R^2 corresponds to a coefficient of determination) and the comparison of the obtained residuals (lower panel) for Mt/R123 dispersions with a constant n_{R123}/m_{Mt} ratio (0.02 mmol g^{-1}) and Mt concentration of 0.209 and 0.418 g dm^{-3} .

The residuals obtained for the dispersion with the lowest Mt concentration (0.209 g dm^{-3}), where the fast process participated in the formation of J-aggregates in a low extent ($c_1/c_{J-agg}^\infty = 0.09$), were negligible compared to the high values of the structured residuals profile observed for the dispersion with the second highest Mt concentration (0.418 g dm^{-3}) for which the c_1/c_{J-agg}^∞ ratio was the highest (0.27) among the whole series of Mt/R123 dispersions with different components concentration.



References

- 1 J. Hrachová, I. Chodák and P. Komadel, *Chem. Pap.*, 2009, **63**, 55–61.
- 2 H. Du, R.-C. A. Fuh, J. Li, L. A. Corkan and J. S. Lindsey, *Photochem. Photobiol.*, 1998, **68**, 141–142.
- 3 Malvern Instruments Ltd., *Zetasizer Nano User Manual*, 2013.
- 4 P. Atkins and J. de Paula, *Atkins' Physical Chemistry*, Eighth Edition, Oxford University Press, Great Britain, 2006.
- 5 L. A. Utracki, M. Sepehr and E. Boccaleri, *Polym Adv Technol*, 2007, 18, 1–37.
- 6 P. Boháč and J. Bujdák, *Clays Clay Miner.*, 2018, **66**, 127–137.
- 7 H. Abdollahi and R. Tauler, *Chemom. Intell. Lab. Syst.*, 2011, **108**, 100–111.
- 8 C. M. Carbonaro, *J.Photochem. Photobiol.*, 2011, **222**, 56–63.
- 9 E. G. McRae and M. Kasha, *J. Chem. Phys.*, 1958, 28, 721–722.
- 10 T. Baranyaiová and J. Bujdák, *Clays Clay Miner.*, 2018, **66**, 114–126.
- 11 T. Baranyaiová and J. Bujdák, *Appl. Clay Sci.*, 2016, **134**, 103–109.
- 12 B. Moore, R. L. Schrader, K. Kowalski and J. Autschbach, *ChemistryOpen*, 2017, **6**, 385–392.
- 13 J. A. B. Ferreira and S. M. B. Costa, *Chem. Phys.*, 2001, **273**, 39–49.
- 14 R. A. Schoonheydt and C. T. Johnston, in *Developments in Clay Science, Handbook of Clay Science, Vol. 1*, eds.: F. Bergaya, B.K.G. Theng, G. Lagaly, Elsevier Ltd., Netherlands, 2006, Chapter 3, 87–113.
- 15 A. H. Gemeay, *J.Colloid Interface Sci.*, 2002, **251**, 235–241.

(int 1)

https://www.julabo.com/sites/default/files/broschuren/CORIO_Refrigerated_and_Heating_Circulators.pdf, p. 25, date of citation 15.07.2021

(int 2)

https://www.malvernpanalytical.com/en/assets/MRK1839_tcm50-17228.pdf, p. 18, date of citation 15.07.2021

(int 3)

<https://mmrc.caltech.edu/HP%208453/Manuals/Agilent%208909%20Peltier.pdf>, p. 15, date of citation: 15.07.2021

(int 4)

<https://www.agilent.com/cs/library/brochures/5989-8680EN.pdf>, p. 3, date of citation 15.07.2021